

UWB Localization via Multipath Distortion

Moshe Uziel and Dana Porrat
The Hebrew University

Abstract—A new method for non line of sight transmitter localization is suggested, based on the effective bandwidth of different multipath components in the UWB channel response. The method essentially relies on the difference in the distortion applied by the channel to early and to late arrivals in the channel impulse response, the early arrivals have a wider effective bandwidth. Localization results on measured channel responses show the superiority of the new method over a method based on a multipath energy detector.

I. INTRODUCTION

Transmitter localization is a problem of interest for a number of important applications. UWB systems offer the potential of accurate localization, as their wide band translates to fine temporal resolution.

Localization in line of sight (LoS) is relatively straight forward, as the direct arrival is also the strongest. The Cramér-Rao Lower Bound for transmitter localization in AWGN was calculated by [1]. [2] and [3] offer pulse detection algorithms for LOS where [2] averages the received signal over a number of frames and correlates the result with the transmitted template, and [3] uses a combination of match filtering and peak search techniques. A two-step ToA estimation algorithm is proposed for LoS in [4] in order to speed up the estimation process. The first step roughly estimates the ToA based on received signal energy. Then, in the second step, a more accurate estimate is achieved using a hypothesis testing approach.

Non line of sight (NLoS) localization is much more complex as the first (direct) arrival may be weak. [5] Addresses the problem of non line of sight (NLoS) localization errors using estimates of the first arrival time and of the strongest arrival. It relies on a non distorted model of the multipath components and shows accuracies of under one meter for terminal separations of up to 12 meters. [6] detects the first path using a time domain generalized maximum likelihood estimation, also based on a channel model with non-distorted multipath components. Its algorithm essentially searches for the earliest arrival. This method is used by [7], that tracks a moving transmitter. [8] compares the ranging errors using delay estimation to those achieved by a technique based on received signal strength. It concludes that additional delay introduced by propagation through walls is a significant source of range error in NLoS indoor environments, and shows localization errors in the range of meters for terminals up to 10 meters apart. [9] estimates the first arrival delay in dense multipath using the generalized likelihood ratio with a channel model based on non-distorted multipath components.

UWB pulse distortion has been modeled in some scenarios [10] and also measured [11]. Interactions with the envi-

ronment (mainly diffractions and reflections) tend to increase the duration of the pulse, [12] shows a reduction of pulse bandwidth for diffracted paths. [13] and [14] concentrate on the adverse effect of pulse distortion on NLoS localization, as the estimation of the time of arrival is hampered by the changes in received pulse shape.

This paper shows how pulse distortion can be used to improve localization performance by assisting in the differentiation between the direct pulse and later arrivals. It suggests a new method for localizing a transmitter in a system that includes the transmitter and a number of receivers in a non line of sight (NLoS) arrangement. The method is based on the observation that the effective bandwidth of the early arrivals is large compared to that of late arrivals. The method is based on two steps: (1) estimating a number of possible arrival times (Tx–Rx separations) at each receiver, and then (2) estimating a number of candidate transmitter positions using the Back Projection method.

II. MODEL

The channel's impulse response can be represented by [10], [15]

$$h(t) = \sum_{l=1}^L h_l(t - \tau_l) \quad (1)$$

where L is the number of significant multipath component, τ_l is the delay of the l^{th} component and its impulse response is $h_l(t)$. The indexing maintains $\tau_1 \leq \tau_2 \leq \dots \leq \tau_L$.

The transmitter emits a pulse $p(t)$ and the received signal is

$$r(t) = h(t) \star p(t) + n(t) = \sum_{l=1}^L h_l(t - \tau_l) \star p(t) + n(t) = \sum_{l=1}^L r_l(t) \quad (2)$$

where \star is convolution, $n(t)$ is noise and $r_l(t)$ are the noisy multipath arrivals at the receiver.

In the following, sampled versions of all signals are used. The sampling rate W is assumed high enough to maintain the significant information in the signals.

III. TIME OF ARRIVAL ESTIMATION

A. The Effective Bandwidth Method

The algorithm is given $r(t)$ and estimates a number of candidate transmitter distances represented as arrival delays.

Step 1: Trim the Signal. There is no need to search over too large or too small delay values. Define T_{\max} as the delay of the absolute maximum of $r(t)$, and d_{before} and d_{after} as the region of interest in terms of transmitter–receiver distances.

The delay span of interest of the received signal is limited to $(T_{\max} - d_{\text{before}}/c, T_{\max} - d_{\text{after}}/c)$, where c is the speed of light in vacuum. Define $r_{1:M}$ as the sampled received signal in the delay span of interest, M is the length of the vector.

Step 2: Windowing. The received signal $r_{1:M}$ is broken into windows of temporal width T , with a temporal shift between consecutive windows of ΔT . Each such window is represented as $r_{(k-1)\Delta TW+1:(k-1)\Delta TW+TW}$ with k between one and a maximum set by the other parameters. The time shift ΔT between windows determines the temporal resolution of the time of arrival estimation, we used $0.04 \text{ cm}/c$ for the results shown below.

Step 3: Effective Bandwidth. For each window of the received signal, zero-pad it with N_z zeroes and calculates its absolute Fourier Transform:

$$R_k(f) = \left| \mathcal{F} \left\{ r_{(k-1)\Delta TW+1:(k-1)\Delta TW+TW}, \text{zeros}_{1:N_z} \right\} \right| \quad (3)$$

Zero padding is required to increase the frequency resolution to $\frac{1}{T+N_z/W}$.

The spectral band of interest $[F_{\min}, F_{\max}]$ is determined by the transmitted pulse bandwidth and by the equipment used to record the received signal. Calculate the effective bandwidth of the k^{th} window:

$$B_k = \frac{\sum_{f=F_{\min}}^{F_{\max}} R_k(f)}{\max_{F_{\min} \leq f \leq F_{\max}} R_k(f)} \quad (4)$$

The effective bandwidth represents the spectral width of the received signal.

Step 4: Estimate time of arrival. Define N as the number of candidate arrival times to be collected, for the results shown below we used $N = 3$. Collect the delay of N maxima of the vector of effective bandwidths B_k into the vector $\tau^B(n)$, $n = 1, \dots, N$. This vector holds estimates of the arrival time of the direct signal from the transmitter.

B. ToA Estimation via Arrival Energy

This section describes a simple time of arrival estimation method [8] used for comparison to the effective bandwidth method suggested above. The first two steps are identical to those described in Section III-A.

Step 3: Calculate Energy. Sum the received signal energy in each window:

$$E_k = \sum_{m=(k-1)\Delta TW+1}^{(k-1)\Delta TW+TW} |r_m|^2 \quad (5)$$

Step 4: Estimate time of arrival. Estimate N candidate time of arrivals as the delay of the N maxima of the vector E_k , collect them into the vector $\tau^E(n)$, $n = 1, \dots, N$.

IV. TIME OF ARRIVAL ESTIMATION RESULTS

A. The Measuring Equipment

The measurement setup consisted of a transmitter based on a pulse generator from Picosecond Pulse Labs, the output pulse had a width of 100 ps , and amplitude $2.7 V_{ptp}$. The signal was fed to an omni-directional transmit antenna via an

amplifier. The transmit antenna was placed on a cart that was moved to different locations for different measurements, but was immobile during each measurement.

The receiver was based on a Agilent DSO81304A sampling oscilloscope (sampling interval 25 ps), it was connected to the receive antenna via an amplifier. The receiver was triggered by the pulse generator, it averaged over 64 measurements. The receive antenna was placed on a rectangular motorized $100 \times 20 \text{ cm}^2$ positioner with sub-millimetric accuracy that was placed on a cart, it was moved between measurements but kept immobile during the collection of each channel response. A computer controlled the location of the receive antenna on the cart and the data collection and management.

B. The Measurements

The measurements were conducted in the Ross Building in the Givat Ram Campus of the Hebrew University of Jerusalem, a standard cement and cement block building from the 1960s. We took 147 channel response measurements with different transmitter and receiver positions in one floor of the building. For each transmitter position the channel response was measured at 5 or 6 receiver positions.

Five receiver positions, collinear at locations $(0:20:100,0)$ cm on the receiver cart, were used with nine transmitter positions, altogether 45 measurements.

Six receiver positions on a rectangle, at positions $(0,0)$, $(0,20)$, $(50,0)$, $(50,20)$, $(100,0)$ and $(100,20)$ cm on the receiver cart were used at three cart locations. The transmitter was located at 17 points, and 6 channel responses were measured for each, altogether 102 measurements. Five of the 26 transmitter positions had line of sight, the other positions were NLoS with one or two walls obstructing the direct path.

C. Time of Arrival Estimation Results

The method described in Section III-A was applied with the following parameter values:

$d_{\text{before}} = \begin{cases} 700 \text{ cm} & cT_{\max} > 750 \\ cT_{\max} - 50 & \text{else} \end{cases}$	Region of Interest [cm]
$d_{\text{after}} = 50$	T_{\max} - delay of maximum of $r(t)$
$T = 5 : 1 : 47 \text{ cm} / c$	Window Size
$\Delta T = 0.04 \text{ cm} / c$	Shift between windows
$N = 3$	Number of ToA Estimates
$N_z = 5000$	Zero Padding
$F_{\min} = 2 \text{ GHz}, F_{\max} = 12 \text{ GHz}$	Spectral Window

The simpler energy-based method described in Section III-B was also applied for reference. Figure 1 shows the average time of arrival estimation error of both methods for LoS and NLoS against bin length T .

Figure 1 shows the average error between the known time of arrival and the best (out of $N=3$) time of arrival estimate, for different values of the window size T . Averaging was done over 147 transmitter–receiver pairs. Time of arrival estimation is significantly less accurate without line of sight. With line of sight between transmitter and receiver, the first arrival is also the strongest and estimation error increases with window size. Line of sight errors are smaller than the window size

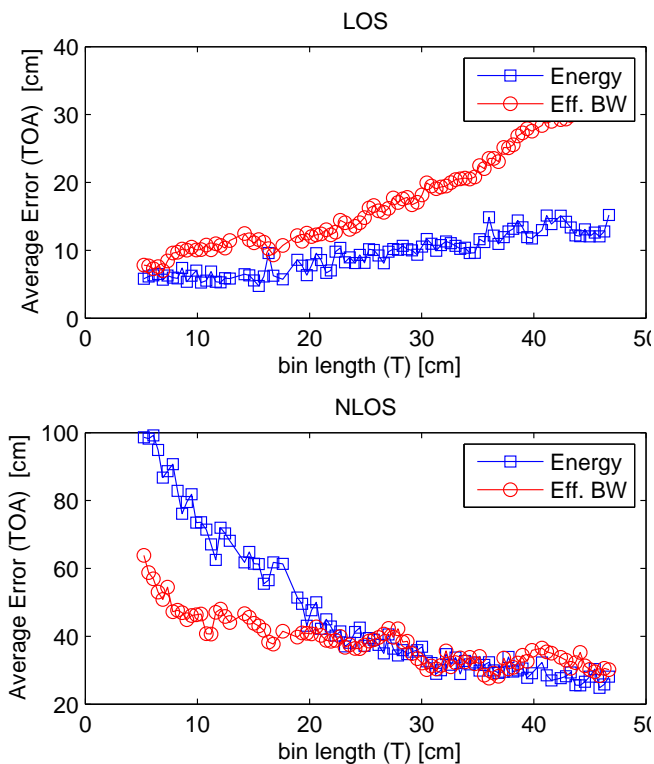


Fig. 1. The average time of arrival estimation error, averaging is taken over all transmitter and receiver locations. The estimation error is taken between the best time of arrival estimate (of three) per each transmitter–receiver pair. The top plot shows line of sight results, the bottom NLoS. Results are shown for two estimation methods based on effective bandwidth and on energy, against window size T multiplied by the speed of light.

(Figure 1). Without line of sight the estimation error decreases as the window size increases.

The effective bandwidth ToA estimation method is superior to the energy based method without line of sight for small values of the window size (below 25 cm).

Localization results in the next section show the advantage of the effective bandwidth method over the energy based method. Accurate localization without line of sight is achieved for low values of the temporal window T , where the effective bandwidth method is superior.

V. LOCALIZATION VIA BACK PROJECTION

Transmitter location is estimated from time of arrival estimates of a number of receivers. Each receiver ($j = 1, \dots, N_R$) outputs an N long vector of candidate times of arrival, marked $\{\tau_j^{B/E}(n)\}_{n=1}^N$ where the superscript B stands for effective bandwidth (Section III-A) and E for energy based (Section III-B). Back Projection [16], [17], [18] is an effective graphical method to estimate transmitter location from the many combinations of candidate arrival times at the different receivers. This method is based on a matrix \mathcal{M} holding a map, where matrix values (map heights) are calculated as a sum of

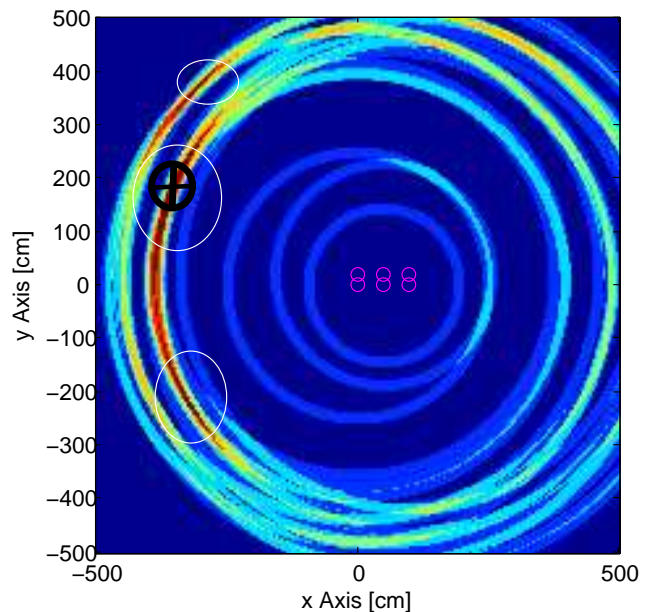


Fig. 2. A Back Projection map generated from measurements with $T=17$ cm/c and $N = 3$, the small circles indicate receiver positions, the transmitter is marked with a cross and a dark circle. The white ellipses indicate the strongest (highest) areas of the map.

circles around each receiver:

$$\mathcal{M}(x, y) = \frac{1}{N_R} \sum_{j=1}^{N_R} A_j \left(\frac{\sqrt{(Rx_j(x) - x)^2 + (Rx_j(y) - y)^2}}{c} \right) \quad (6)$$

$Rx_j(x)$ and $Rx_j(y)$ stand for the (x, y) position of receiver j . The function $A_j(\cdot)$ describes circles at radii determined by the estimated arrival times at receiver j :

$$A_j(t) = \sum_{n=1}^N \exp \left\{ -\frac{t^2}{2T^2} \right\} \text{rect} \left(\frac{t - \tau_j(i)}{T} \right) \quad (7)$$

The circles have a Gaussian profile with parameter T , trimmed to width T . The function $\text{rect}(\cdot)$ is a rectangle of unit height between $-1/2$ and $1/2$. An example of a back projection map generated from measurements is shown in Figure 2.

The map is thresholded, and results in a number of candidate areas of transmitter location. Our results yielded up to 5 such areas per transmitter and receiver cart locations.

The next step is the calculation of the weighted center of each such area, using the map height as weight, and the selection of a single estimate of the transmitter location, that takes into account the physical limitations of the environment.

VI. LOCALIZATION RESULTS

Based on time of arrival estimates from Section IV-C a back projection map was generated and the transmitter location was estimated. Figure 3 presents the averaged localization error with and without line of sight, where the best of up to 5 location estimates was used. Averaging was done over

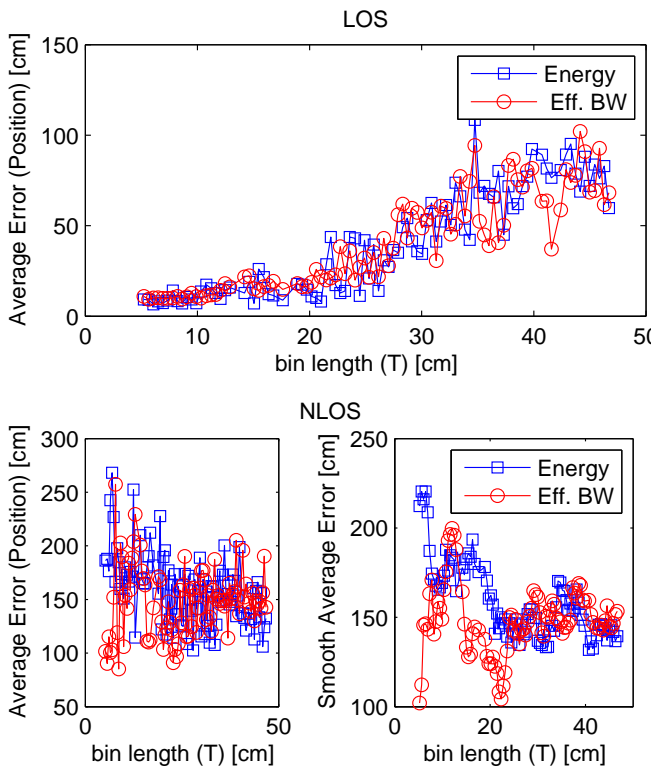


Fig. 3. Average localization error for line of sight (top) and without line of sight (bottom left). The location estimate was chosen as the best of up to 5 estimates generated from the back projection map. Results are averaged over transmitter and receiver cart locations, and shown for the effective bandwidth method and for the energy based method of time of arrival estimation. The horizontal axis holds window size. The bottom right graph is a 5-point smoothed version of the NLoS results from the bottom left pane.

transmitter and receiver cart locations and the results are shown against window size. Localization performance in line of sight appear similar for the effective bandwidth method and the energy based method, although the energy based method gives better time of arrival estimates (Figure 1). The reason is that the window size T limits the achievable accuracy in this case.

Non line of sight results (Figure 3, bottom right pane) show the superiority of the effective bandwidth method. Best localization results are achieved with the effective bandwidth, with a small window (around 25 cm).

VII. CONCLUSION

This paper suggests a new method for non line of sight transmitter localization, based on the observation that the bandwidth of multipath components is larger for early arrivals. The time of arrival estimation method was tested on measured data and compared to a method based on energy detection, with comparable errors. The benefit of the new method is

apparent in localization performance, where the effective bandwidth method offers superior performance.

REFERENCES

- [1] S. Gezici, Z. Tian, G. Giannakis, H. Kobayashi, A. Molisch, H. Poor, and Z. Sahinoglu, "Localization via ultra-wideband radios: a look at positioning aspects for future sensor networks," *Signal Processing Magazine, IEEE*, vol. 22, no. 4, pp. 70 – 84, july 2005.
- [2] W. C. Chung and D. Ha, "An accurate ultra wideband (uwb) ranging for precision asset location," in *Ultra Wideband Systems and Technologies, 2003 IEEE Conference on*, nov. 2003, pp. 389 – 393.
- [3] Z. Low, J. Cheong, C. Law, W. Ng, and Y. Lee, "Pulse detection algorithm for line-of-sight (LOS) UWB ranging applications," *Antennas and Wireless Propagation Letters, IEEE*, vol. 4, pp. 63 – 67, 2005.
- [4] S. Gezici, Z. Sahinoglu, A. Molisch, H. Kobayashi, and V. Poor, "A two-step time of arrival estimation algorithm for impulse radio ultra wideband systems," in *Proc. 13th European Signal Processing Conference*, 2005, pp. 4–8.
- [5] B. Denis, J. Keignart, and N. Daniele, "Impact of NLOS propagation upon ranging precision in UWB systems," in *Ultra Wideband Systems and Technologies, 2003 IEEE Conference on*, nov. 2003, pp. 379 – 383.
- [6] J.-Y. Lee and R. Scholtz, "Ranging in a dense multipath environment using an UWB radio link," *Selected Areas in Communications, IEEE Journal on*, vol. 20, no. 9, pp. 1677 – 1683, dec 2002.
- [7] F. Evennou, F. Marx, and S. Nacivet, "An experimental TDOA UWB location system for NLOS environments," in *Vehicular Technology Conference, 2005. VTC-2005-Fall. 2005 IEEE 62nd*, vol. 1, sept., 2005, pp. 420 – 423.
- [8] Z. Irahauten, G. Bellusci, G. J. Janssen, H. Nikookar, and C. Tiberius, "Investigation of UWB ranging in dense indoor multipath environments," in *Communication systems, 2006. ICCS 2006. 10th IEEE Singapore International Conference on*, oct. 2006, pp. 1 –5.
- [9] C. Mazzucco, U. Spagnolini, and G. Mulas, "A ranging technique for UWB indoor channel based on power delay profile analysis," in *Vehicular Technology Conference, 2004. VTC 2004-Spring. 2004 IEEE 59th*, vol. 5, may 2004, pp. 2595 – 2599 Vol.5.
- [10] R. C. Qiu, H. Liu, and X. Shen, "Ultra-wideband for multiple access communications," *IEEE Communications Magazine*, vol. 43, no. 82, pp. 80–87, Feb 2005.
- [11] M. Di Renzo, R. Buehrer, and J. Torres, "Pulse shape distortion and ranging accuracy in uwb-based body area networks for full-body motion capture and gait analysis," in *Global Telecommunications Conference, 2007. GLOBECOM '07. IEEE*, nov. 2007, pp. 3775 –3780.
- [12] L. Ma, A. Duel-Hallen, and H. Hallen, "Physical modeling and template design for UWB channels with per-path distortion," in *Military Communications Conference, 2006. MILCOM 2006. IEEE*, oct. 2006, pp. 1 –7.
- [13] M. Jing, Z. Nai-tong, and Z. Qin-yu, "IR-UWB waveform distortion analysis in NLOS localization system," *Information Technology Journal*, vol. 9, no. 1, pp. 139–145, 2010.
- [14] C. Zhou and R. Qiu, "Pulse distortion caused by cylinder diffraction and its impact on UWB communications," in *Ultra-Wideband, The 2006 IEEE 2006 International Conference on*, sept. 2006, pp. 645 –650.
- [15] R. C. Qiu, C. Zhou, and Q. Liu, "Physics-based pulse distortion for ultra-wideband signals," *IEEE Trans. on Vehicular Technology*, vol. 54, no. 5, pp. 1546–1555, Sept 2005.
- [16] R. Zetik, J. Sachs, and R. Thoma, "Imaging of the propagation environment by UWB channel sounding," in *General Assembly Int. Union of Radio Science (URSI)*, Oct. 2005.
- [17] —, "Modified cross-correlation back projection for UWB imaging: numerical examples," in *Ultra-Wideband, 2005. ICU 2005. 2005 IEEE International Conference on*, sept. 2005, p. 5 pp.
- [18] —, "UWB localization - active and passive approach [ultra wideband radar]," in *Instrumentation and Measurement Technology Conference, 2004. IMTC 04. Proceedings of the 21st IEEE*, vol. 2, may 2004, pp. 1005 – 1009 Vol.2.